A New Vertical Reduction Model for Enhancing the Interpolation Accuracy of VMF1/VMF3 Tropospheric Delay Products

Peng Sun[1], Kefei Zhang[1,2], Dantong Zhu[3], Shuangshuang Shi[4], Xuexi Liu[1], Dongsheng Zhao[1], Minghao Zhang[1], Suqin Wu[1]

[1] School of Environment Science and Spatial Informatics, China University of Mining and Technology, Xuzhou 221116, China

[2] Satellite Positioning for Atmosphere, Climate and Environment (SPACE) Research Centre, RMIT University, Melbourne VIC 3001, Australia

[3] College of Surveying and Geo-Informatics, North China University of Water Resources and Electric Power, Zhengzhou 450000, China

[4] Shandong Provincial Key Laboratory of Water and Soil Conservation and Environmental Protection, College of Resources and Environment, Linyi University, Linyi 276000, China

Correspondence to: Kefei Zhang (profkzhang@cumt.edu.cn); Shuangshuang Shi (shshshi@whu.edu.cn)

Abstract. Grid-wise Vienna Mapping Functions 1 (VMF1) and Vienna Mapping Functions 3 (VMF3) tropospheric products are widely used to interpolate the a priori zenith hydrostatic delay (ZHD) and zenith wet delay (ZWD) over GNSS (Global Navigation Satellite Systems) stations for the mitigation of tropospheric delays contained in GNSS observations. Since these two products provide ZHD and ZWD values only for the ground surface at global grid points, the ZHD and ZWD at the four grid points nearest to a GNSS site used to interpolate for the GNSS site need to be reduced to the same height of the GNSS station before a horizontal interpolation (e.g., bilinear interpolation) is implemented. However, the accuracy of the officially recommended reduction model may not be as good as desired, especially in the case that the height of the GNSS site largely differs from that of the four ground grid points. To address this, a new vertical reduction model for reducing the ZHD and ZWD at the height of grid points to a target height was developed. The sample data for the modelling were the 10-year (2010–2019) ZHD and ZWD profiles over grid points obtained from ERA5 monthly averaged reanalysis data, while the 3-year (2020–2022) radiosonde profiles and the IGS (International GNSS Service) site-wise zenith tropospheric delay (ZTD) products were used to evaluate the new model. Results demonstrated that the accuracy of ZHD, ZWD, and consequently ZTD values interpolated from VMF1/VMF3 products and the new model considerably improved compared to traditional methods, especially at the target sites that have large height differences from its closest VMF grid points. This improvement has significance for those applications that need to use tropospheric delay corrections, e.g. in GNSS positioning and GNSS meteorology for a desired accuracy

1 Introduction

Tropospheric delay arises when electromagnetic waves propagate through the Earth's atmosphere and are refracted by neutral gases, which is defined as:

$$TD = 10^{-6} \int N \, ds + (\int ds - L) \tag{1}$$

where the first term represents the delay caused by the change in signal velocity along the actual (bent) propagation path s; the second term accounts for the geometric path difference along the straight satellite–receiver line L; N is the atmospheric refractivity (dimensionless):

$$\begin{aligned} N &= k_1 \cdot \frac{P_d}{T} + (k_2 \cdot \frac{e}{T} + k_3 \cdot \frac{e}{T^2}) \\ &= k_1 \cdot \frac{P}{T} + (k_2^{'} \cdot \frac{e}{T} + k_3 \cdot \frac{e}{T^2}) \\ &= N_h + N_{nh} \end{aligned} \tag{2}$$

where k_1, k_2, k_3 are three refractivity constants (Rüeger, 2002; Thayer, 1974); P_d and e are atmospheric pressures (in hPa) resulting from dry air and water vapor, respectively; P is the total atmospheric pressure ($P = P_d + e$); T is the atmospheric temperature (in K); N_h and N_{nh} are hydrostatic and non-hydrostatic part of the refractivity, respectively. k_2' is a constant related to k_1 and k_2:

$$k_2^{'} = k_2 - k_1 \frac{R_d}{R_v} \tag{3}$$

where R_d and R_v are the specific gas constants for dry air and water vapor, respectively. $R_d = R / M_d$, $R_v = R / M_v$, where R is the universal gas constant (8.3143 J/K/mol); M_d (28.9644 g/mol) and M_w (18.0152 g/mol) are the molar mass of dry air constant and water, respectively.

The tropospheric delay is one of the major error sources embedded in observations of space geodetic techniques, such as GNSS (Global Navigation Satellite Systems) and VLBI (Very Long Base-line Interferometry). The second term in Eq. (1), which represents the geometric path change, is typically quite smaller than the first term (usually less than 0.1 mm for elevation angles above 57°). Moreover, the bending effect is generally accounted for using advanced mapping functions (see Eq.(5)) (Möller and Landskron, 2019; Nafisi et al., 2012) . Therefore, most research efforts focus on modelling the first term in Equation (1), which dominates the total delay. As a convention, the zenith tropospheric delay (ZTD) is widely used in GNSS and VLBI data processing:

$$ZTD = \int N_h \, dh + \int N_{nh} \, dh = ZHD + ZWD \tag{4}$$

where ZHD and ZWD are zenith hydrostatic delay and zenith non-hydrostatic delay (also known as zenith wet delay (ZWD)), respectively. Then a slant tropospheric delay can be modelled using ZHD, ZWD together with mapping functions (Chao, 1974; Chen and Herring, 1997; Niell, 1996):

$$TD = ZHD \cdot mf_h + ZWD \cdot mf_w + \Delta T_{grad} \tag{5}$$

where mf_h and mf_w are the mapping functions for the hydrostatic and non-hydrostatic part of the tropospheric delay, respectively; ΔT_{grad} is the tropospheric gradient, which is caused by the azimuthal asymmetry of the troposphere.

Given the distinct dynamic characteristics of the ZHD and ZWD, GNSS data processing typically applies a correction for the ZHD using external models or products, while treating the ZWD as an unknown parameter to be estimated. Due to

differences between the hydrostatic and wet mapping functions, the error in ZHD cannot be absorbed into the estimated ZWD completely, This discrepancy can subsequently degrade the accuracy of both the ZTD and station height estimates (Boehm et al., 2006; Tregoning and Herring, 2006; Kouba, 2009). Moreover, accurate ZHD is crucial in GNSS meteorology, where ZTD is converted to precipitable water vapor (Bevis et al., 1992; Wang et al., 2017; Zhu et al., 2024) . A 1 cm error in ZHD can introduce an error of approximately 1.5 mm in the retrieved PWV. For ZWD , pre-obtained values can be used directly to correct the wet delay or treated as pseudo-observations to constrain the estimation of the wet delay, thereby accelerating the convergence of precise point positioning (PPP) solutions (Sun et al., 2021a). Therefore, improving the accuracy of ZHD and ZWD has been a long-standing global effort in the advancement of space geodetic data processing.

The zenith hydrostatic delay (ZHD) can be modeled with high accuracy using the Saastamoinen model, provided that in-situ atmospheric pressure (P) measurements are available (Davis et al., 1985; Saastamoinen, 1972):

$$ZHD = \frac{0.0022768P}{f(\varphi, H)} = \frac{0.0022768P}{1 - 0.00266\cos(2\varphi) - 0.00028H} \tag{6}$$

where φ and H are the latitude (in radians) and height (in km) of the GNSS site, respectively. Although the ZWD can also be calculated using empirical models such as the Askne-Nordius model (Askne and Nordius, 1987), which relies on in-situ meteorological measurements (e.g., water vapor pressure), its accuracy is generally lower than that of the ZHD model. This is primarily because water vapor exhibits high spatial variability, even when precise in-situ measurements are available(Chen and Liu, 2016).

Since most GNSS stations are not mounted with meteorological sensors and it is computationally complex for real-time GNSS users to process forecasted numerical weather model (NWM) data to obtain the atmospheric parameters, empirical tropospheric delay models are widely used alternatives. Among the most commonly adopted models are the UNB3m model (Leandro et al., 2006) developed by the University of New Brunswick(UNB) and the Global Pressure and Temperature (GPT) model series developed by the Vienna University of Technology (TU Wien). These models operate independently of external meteorological inputs and empirically estimate atmospheric parameters (such as atmospheric pressure, water vaper pressure, temperature, etc.) based solely on a given location and time. The UNB3m model uses lookup tables that provide the mean and annual amplitude of meteorological variables at mean sea level, facilitating tropospheric delay computation through standardized vertical reduction models. Boehm et al. (2007) introduced the first version of the GPT model, which represents global atmospheric pressure and temperature using spherical harmonics. Its successor, GPT2 (Lagler et al., 2013) advanced the GPT series by implementing a global 5°×5° grid and characterizing atmospheric pressure, temperature, temperature lapse rate, and water vapor pressure by accounting for their mean, annual, and semi-annual harmonics. The GPT2w model (Böhm et al., 2015) refined this framework by incorporating additional parameters and increasing the resolution to 1°×1°. The GPT3 (Landskron and Böhm, 2018) integrated an empirical gradient model while maintaining the other meteorological parameters consistent with GPT2w. Both the UNB3m and GPT model series furnish meteorological parameters at a single reference level (either mean sea level or Earth's surface), necessitating their vertical propagation to the desired elevation. To enhance the accuracy of tropospheric delay modelling, recent studies have introduced more advanced modelling techniques that better

describe the height-dependent variability of atmospheric parameters (Huang et al., 2023; Jiang et al., 2024; Li et al., 2018; Sun et al., 2023). Nevertheless, while these empirical models can predict atmospheric parameters with reasonable accuracy, they are fundamentally limited to capturing long-term average variations, primarily annual and semi-annual cycles. As a result, their predictive accuracy is inherently constrained by the atmosphere's continuous and often abrupt variability, particularly for rapidly fluctuating parameters such as air temperature and water vapor pressure (Wang et al., 2017; Xia et al., 2023).

Fortunately, the tropospheric delay can also be obtained from grid-wise Vienna Mapping Functions 1 (VMF1) (Boehm et al., 2006, 2009) and Vienna Mapping Functions 3 (VMF3) (Landskron and Böhm, 2018) products provided by TU Wien. The grid-based VMF1 product has a horizontal resolution of 2.5°×2°, while the VMF3 product offers resolutions of 1°×1° and 5°×5°. For each grid point, he ZHD, ZWD, and mapping function coefficients are computed at four epochs (0, 6, 12, 18 UTC) per day using NWM data from the European Centre for Medium-Range Weather Forecasts (ECMWF). These products allow tropospheric delays for any specific time and location to be obtained via interpolation from surrounding grid points. Two types of NWM data are used to generate the VMF1/VMF3 products, i.e., ECMWF OPERATIONAL NWM for VMF1_OP and VMF3_OP, and ECMWF FORECAST NWM for VMF1_FC and VMF3_FC. In addition, some other VMF1-like products are also publicly available for users (Santos, 2011; Zus et al., 2015).

Recent studies have shown that the accuracy of the tropospheric delays obtained from the grid-wise VMF1 and VMF3 products are significantly better than those predicted by the above-mentioned empirical models (Sun et al., 2021b; Yang et al., 2021). Prior to the release of VMF3, the VMF1 product was highly recommended for GNSS data processing (Kouba, 2008). Yao et al. (2018b) evaluated the ZTD predicted by VMF1_FC using references from IGS (International GNSS Service) final ZTD products and results demonstrated a mean root-mean-square (RMS) of 1.83 cm. Yuan et al. (2019) assessed the performance of VMF1_FC in real-time precise point positioning (PPP) and found that the accuracy of PPP-derived positions and ZTDs was superior when using ZHD values from VMF1_FC compared to empirical models. The VMF3 product, offering resolutions of 1° × 1° and 5° × 5°, have become available since 2018, and its associated mapping function has been shown to outperform that of VMF1 (Landskron and Böhm, 2018). Sun et al. (2021a) utilized ZWD values predicted by VMF3_FC (1°×1°) as a pseudo-observation to constrain the ZWD parameter in real-time single-frequency (SF) PPP, demonstrating that the convergence time of SF-PPP was significantly shortened. Yang et al. (2021) evaluated the accuracy of the ZHD and ZWD values predicted by VMF3_OP across China using reference data from ERA5 reanalysis. Sun et al.(2021b) evaluated the accuracy of the ZHD predicted by VMF1_FC and VMF3_FC using 3-year surface atmospheric pressures measured at 443 globally distributed radiosonde stations and results showed that the mean RMSE of the ZHD values predicted by VMF1_FC, VMF3_FC (5°×5°) and VMF3_FC (1°×1°) at all the 443 stations were 5.9, 5.4, and 4.3 mm, respectively.

While ZTD values derived from VMF1 and VMF3 products generally exhibit superior accuracy compared to those derived from empirical tropospheric models, notable errors in ZHD and ZWD under certain conditions have been reported in several studies(Sun et al., 2021b; Yang et al., 2021; Yao et al., 2018b). In particular, the RMSE of ZHD estimated using grid-wise VMF1/VMF3 data with the officially recommended interpolation method can reach up to 5 cm when compared with reference ZHD values obtained from radiosonde measurements in certain regions(Sun et al., 2021b). Similarly, the RMSE of

ZWD can also reach substantial magnitudes(Sun et al., 2021a; Yang et al., 2021). These findings highlight the potential limitations of existing interpolation methods, particularly in regions characterized by complex terrain. To address this issue and improve the accuracy of ZTD interpolated from VMF1/VMF3 products, this study re-evaluates the conventional interpolation strategy and introduces a new vertical reduction model. This model provides grid-wise vertical reduction coefficients for ZHD and ZWD at each VMF grid point, enabling more accurate height-related adjustments prior to horizontal interpolation. The methodology and data utilized in this research are presented first, followed by test results, their analyses, and discussion. Conclusions are summarized in the final section.

2 Data Sources

2.1 ERA5 monthly averaged reanalysis data

ERA5 reanalysis data are the state-of-the-art atmospheric reanalysis data provided by the ECMWF. In this contribution, the 10 years (2010–2019) of ERA5 monthly averaged reanalysis data, including geopotential, temperature and water vapor pressure at 37 pressure levels over the grid points of VMF1 and VMF3 products were selected as the samples for the development of the new ZTD vertical reduction model. To adapt to geodetic applications, the geopotential heights were converted to ellipsoidal heights using the transformation equations described by Nafisi (2012).

2.2 Radiosonde data

For the evaluation of the newly developed ZHD and ZWD vertical reduction models, atmospheric profiles from 608 radiosonde stations in the 3-year period of 2020–2022 were selected for the calculation of references. The selection was based on the criterion that the station observed at least 500 valid profiles during the 3-year period to ensure temporal continuity. The geographical distribution of these finally selected stations is illustrated in Fig. 1(a). The reference ZHD and ZWD were obtained using discrete integration form of Eq. (4) (Andrei and Chen, 2009; Askne and Nordius, 1987):

$$\begin{aligned} ZHD &= \sum N_h dh \\ ZWD &= \sum N_{nh} dh \end{aligned} \tag{7}$$

2.3 GNSS-ZTD data

ZTD products in the 3-year period of 2020–2022 at 394 IGS stations were used to evaluate the new ZHD and ZWD vertical reduction models. A rigorous quality control procedure was implemented to ensure the quality of these reference ZTDs. Initially, the IGS-ZTD time series, originally at 5-mins intervals, was resampled to a 2-hour interval. To mitigate the impact of known midnight discontinuities, present in the IGS-ZTD time series, only odd-numbered UTC epochs (i.e., 1, 3, ..., 23) were retained. Subsequently, epochs with a standard deviation exceeding 4 mm, as indicated within the IGS-ZTD products, were excluded. Consequently, those stations that had less than 5000 ZTD epochs were removed., and the number of the remained stations was 394, see the geographical distribution of these stations in Fig. 1(b).

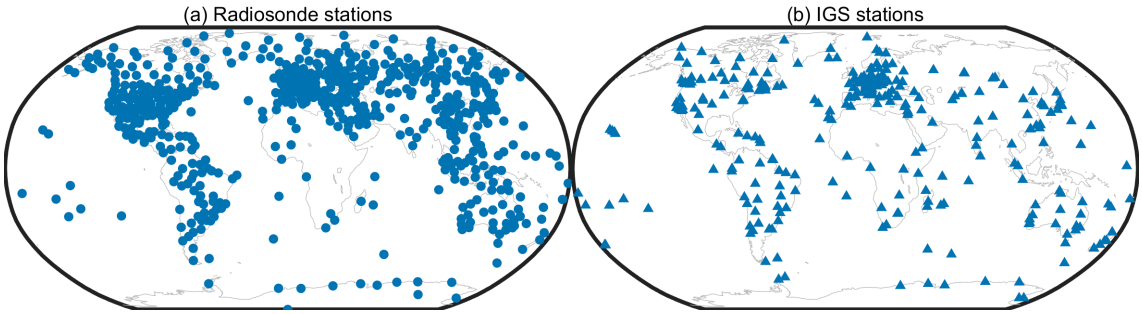

Figure 1. Geographical distribution of (a) 608 radiosonde stations and (b) 394 GNSS stations selected for the evaluation of the new model

3 Methodology

3.1 Officially recommended ZTD interpolation method

The officially recommended ZTD interpolation method is examined in this section for the analysis of improvements to be made in the accuracy of VMF1/VMF3-predicted ZTD. Its procedure is as follows.

[1]. Identifying the four ground grid points surrounding the target point S (see Fig. 2) provided in the VMF1and VMF3 products, see points A~D. Then, for each grid point, the following procedure is performed.

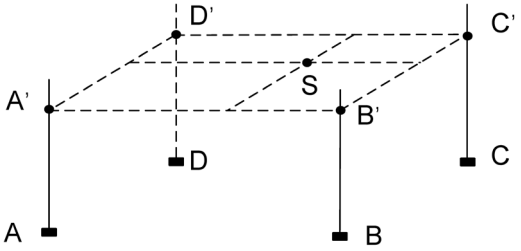

Figure 2 ZHD and ZWD at the position of S are obtained by an interpolation of the ZHD and ZWD values at the four ground grid points surrounding S (A to D), then reduced to the height of S (*A'~D'*).

[2]. Performing a linear interpolation for the ZHD and ZWD values of the grid point in the temporal domain: data from the two neighbouring epochs (selected from 0, 6, 12, 18 UTC) that are closest to *S* are used in the interpolation, and the interpolated results are denoted by ZHD_0 in Eq. (8) and ZWD_0 in Eq. (10) since they are the ground surface value at one of A ~ D.

[3]. Using an inverse process of Eq. (6) to calculate the ground atmospheric pressure of the grid point:

$$P_0 = \frac{ZHD_0[1-0.00266\cos(2\varphi)-0.00028h_0]}{0.0022768} \tag{8}$$

where P_0 and h_0 are the ground atmospheric pressure and height of the grid point, respectively.

[4]. Reducing P_0 to the height of *S* using the following vertical atmospheric pressure reduction model (Kouba, 2008):

$$P = P_0\left(1 - 0.0000266\Delta h\right)^{5.225} \tag{9}$$

where P is the reduced atmospheric pressure at the height of S (A'~D'); 0.0000266 is an empirical decay parameter for atmospheric pressure; Δh is the difference between the target and reference heights, i.e. $\Delta h_{AA'}$, $\Delta h_{BB'}$, $\Delta h_{CC'}$, $\Delta h_{DD'}$.

[5]. Using Eq. (6) with the input of P obtained in Eq. (8) to obtain reduced ZHD for the grid point.

[6]. Using ZWD_0 (i.e., ground) and the following model to obtain ZWD for the height of S for the grid point:

$$ZWD = ZWD_0 \bullet \exp\left(\frac{-\Delta h}{2000}\right) \tag{10}$$

[7]. Repeating steps [2]-[6] for all the four points (A'~D'), then using the four reduced ZHD and ZWD values and the bilinear interpolation in the spatial domain to obtain the interpolated ZHD and ZWD for the position of S.

3.2 GPT2w-based ZTD reduction method

It is noted that in Eq. (9), a fixed empirical value 0.0000266 is used for the atmospheric pressure decay parameter on a global scale. However, due to the spatio-temporal variations in atmospheric pressure (Wang et al., 2022; Zhang et al., 2021a), the vertical reduction model may not perform well. Therefore, taking into account the spatio-temporal variations in atmospheric pressure models is most likely to improve their accuracy. For example, Eq. (9) can be replaced with:

$$P = P_0\left(1 - \frac{\beta}{T_0}\Delta h\right)^{\frac{g_m \bullet M_d}{R \bullet \beta}} \tag{11}$$

where T_0 is the temperature (in K) at the reference height; β is the temperature lapse rate; g_m is the mean gravitational acceleration. The accuracy of T_0 and β determines the accuracy of the vertical reduction function. Fortunately, these two values can be obtained from empirical models e.g. GPT2w. Zhang et al. (2021b) utilized GPT2w-predicted atmospheric temperature and its lapse rate as the input of Eq. (11) for the vertical reduction to the ZHD provided by VMF1/VMF3-like products, and test results in the Tibetan Plateau region showed significant improvements.

In this research, the water vapor decrease factor (λ) predicted by GPT2w was applied to the vertical reduction for the ZWD provided in grid-wise VMF1/VMF3 products using the following ZWD decay function given by Dousa (2014):

$$ZWD = ZWD_0\left(1 - \frac{\beta}{T_0}\Delta h\right)^{\frac{(\lambda+1) \bullet g_m}{R_d \bullet \beta}} \tag{12}$$

3.3 A new ZTD reduction method for VMF1/VMF3 products

If a constant temperature lapse rate ($\beta = 0.0065$ K/m) is utilized, the exponential term of Eq. (11). can be simplified as(Yao et al., 2018a):

$$P = P_0\left[1 - \tau\left(h - h_0\right)\right]^{5.256} \tag{13}$$

where $\tau = \beta / T_0$. Since the denominator part of Eq. (6), i.e., f (φ, H) in Eq. (6), is close to 1, the specific value of the ZHD at height h above the reference height can be simplified as:

$$\frac{ZHD}{ZHD_0}=\frac{P_0\left[1-\tau\left(h-h_0\right)\right]^{5.256}}{P_0} \tag{14}$$

Then the ZHD at height h can be obtained by:

$$ZHD=ZHD_0\left[1-\tau\left(h-h_0\right)\right]^{5.256} \tag{15}$$

The ZWD decay function proposed by Dousa (2014) was utilized in this study:

$$\frac{ZWD}{ZWD_0}=\left(\frac{P}{P_0}\right)^{\gamma+1} \tag{16}$$

where γ is the ZWD decay parameter.

Substituting Eq. (13) into Eq. (16) leads:

$$\frac{ZWD}{ZWD_0}=\left[1-\tau\left(h-h_0\right)\right]^{5.256(\gamma+1)} \tag{17}$$

Thus

$$ZWD=ZWD_0\left[1-\tau\left(h-h_0\right)\right]^{5.256(\gamma+1)} \tag{18}$$

In this study, τ and γ for each of VMF1/VMF3 grid points were modeled using the following procedure:

[1]. For the spatial domain, τ and γ at the ground surface of the grid point for the 120 months in the 10-year period of 2010–2019 were fitted using the ERA5 monthly averaged reanalysis data mentioned above.

[2]. For the temporal domain, the seasonal variation trends of τ and γ at the grid point fitting the above 120 monthly averaged τ and γ values were modelled by:

$$t=t_0+A_1\cos\left(\frac{DOY-d_1}{365.25}2\pi\right)+A_2\cos\left(\frac{DOY-d_2}{365.25}4\pi\right) \tag{19}$$

where t_0 is the mean of the parameter (i.e., either τ or γ); A_1 and A_2 are the amplitudes of annual and semi-annual variation of the parameter, respectively; d_1 and d_2 are the day of year (DOY) corresponding to their initial phase. Then the ZHD and ZWD at height h can be obtained using Eq. (15) and Eq. (18), respectively.

4 Results and discussion

To compare the accuracies of the standard and alternative vertical reduction models for reducing the ground surface ZHD and ZWD from the grid reference height to GNSS station heights, the following three schemes were tested using ZHD and ZWD data obtained from grid-wise VMF1/VMF3 products.

1) Scheme 1: for the officially recommended reduction methods, which utilizes fixed empirical decay parameters, corresponding to Eq. (9) for ZHD and Eq. (10) for ZWD.

2) Scheme 2: for the temperature-dependent pressure decay model (Eq. (11)) and the exponential ZWD decay model (Eq. (12)). The required atmospheric variables, including temperature (T_0), temperature lapse rate (β), and water vapor decay coefficient (λ), are predicted by the GPT2w model.

3) Scheme 3: for the new vertical reduction model developed in this research, i.e., Eq. (15) for ZHD and Eq. (18) for ZWD.

The RMSE was used to measure the overall accuracy of results obtained from the above three schemes:

$$RMSE = \sqrt{\frac{1}{n}\sum_{i=1}^{n}\left(ZTD_{VMF,i} - ZTD_{ref,i}\right)^2} \tag{20}$$

where ZTD_{VMF} and ZTD_{ref} are the VMF-based ZTD (or ZHD, ZWD) and the reference ZTD (or ZHD, ZWD), respectively. It should be noted that only the forecast VMF1/VMF3 products were utilized for the model evaluation since only these two products could be adapted to real-time GNSS data processing and real-time retrieval of PWV in GNSS meteorology.

4.1 Using radiosonde-ZTD as reference

In this section the ZHD and ZWD obtained from the 3-year (2020–2022) radiosonde profiles at eight pressure levels at the aforementioned 608 radiosonde stations were used as the reference.

Figure 3(a) (the top row) shows each scheme's mean RMSE of ZHD interpolated from VMF1 and VMF3 (with three spatial resolutions) at each pressure level in the 3-year period at all the 608 stations. We can see that Scheme 2 outperforms Scheme 1 at the three lowest levels (i.e. 1000, 925 and 850 hPa). However, at all the rest height levels Scheme 2 (blue) results are much worser than the other two, and the higher, the worser of its accuracy. Moreover, results from Scheme 3 (for the new model) were significantly better than the other two and its accuracies at different levels had little differences.

From Figure 3(b), which is for the results of the interpolated ZWD, we can see that Scheme 3 is also the best performer. Furthermore, at low levels, e.g. below 500 hPa, where the water vapor content mainly concentrates, Scheme 1 (black) is the worst, and Schemes 2 and 3 perform similarly. However, at the rest four levels (high), Schemes 1 and 3 had little differences, while Scheme 2 is the worst.

To summarize the above results, Scheme 3 (i.e. our new model) is the best in reducing the ZWD obtained from the grid-wise VMF1/VMF3 products, while Scheme 2 may offer an improved result only at low-altitude pressure levels in comparison with Scheme 1 (the officially recommended one).

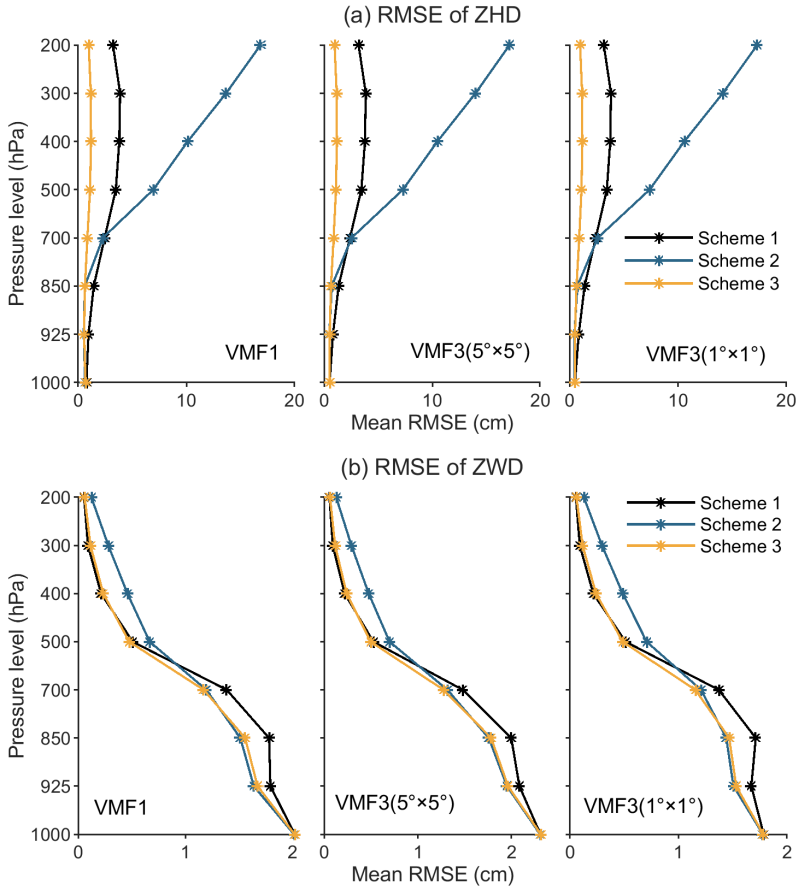

Figure 3 Mean RMSE of the (a) ZHD and (b) ZWD interpolated from VMF1_FC and VMF3_FC for each scheme at each pressure level in the 3-year (2020 – 2022) period at 608 radiosonde stations

4.2 Using IGS-ZTD as reference

ZTD values at the aforementioned 394 IGS stations in the 3-year period studied were also used as the reference to evaluate the performance of the above three schemes. As introduced at the beginning of Section 4, these schemes represent different approaches to interpolating ZTD from gridded VMF data to station height.

Table 1 lists the mean, maximum and minimum RMSE values of the interpolated ZTDs from each scheme. One can observe that the maximum RMSE from Scheme 3 is significantly lower than those from Schemes 1 and 2, indicating that the proposed model significantly enhances the interpolation accuracy of ZTD.

It should be noted that the IGS ZTD values are for ground surface and most IGS stations are located in relatively flat terrain, thus the mean RMSE of Scheme 3 was not significantly smaller than that of the other two schemes. However, for those stations that substantially higher or lower that its adjacent VMF grid points, the accuracy of interpolated ZTD for these stations was significantly improved. As an example, Figure 4 shows the time series of errors in VMF1/VMF3 predicted ZTD at the IQQE

(IGS) station and the IGS final ZTD product was used as the reference. The figure indicates a significant effect of height differences between a GNSS station and its neighboring VMF1/VMF3 grid points on the interpolated ZTD (ZHD+ZWD). Note that the IQQE (IGS) station is located in Iquique, Chile，lies to the west of the Andes Mountains, thus this station exhibits substantial differences in height compared to its surrounding closest VMF1/VMF3 grid points: the maximum height differences reach 1562 m for VMF1, 4632 m for VMF3 (5°×5°), and 2750 m for VMF3 (1°×1°). These height differences led to large errors in the ZTD resulting from Schemes 1 and 2, while the ZTD resulting from Scheme 3 was significantly improved.

Table 1 Mean, minimum and maximum RMSE (in cm) of ZTD resulting from each scheme in the 3-year period studied at 394 IGS stations.

Schemes	VMF1			VMF3(5°×5°)			VMF3(1°×1°)		
	min	mean	max	min	mean	max	min	mean	max
1	0.51	1.90	**6.79**	0.90	2.20	**6.05**	0.80	1.60	**3.16**
2	0.69	1.82	**8.25**	0.52	2.21	**29.67**	0.52	1.55	**5.45**
3	0.76	1.78	**3.89**	0.61	2.05	**4.45**	0.62	1.51	**2.84**

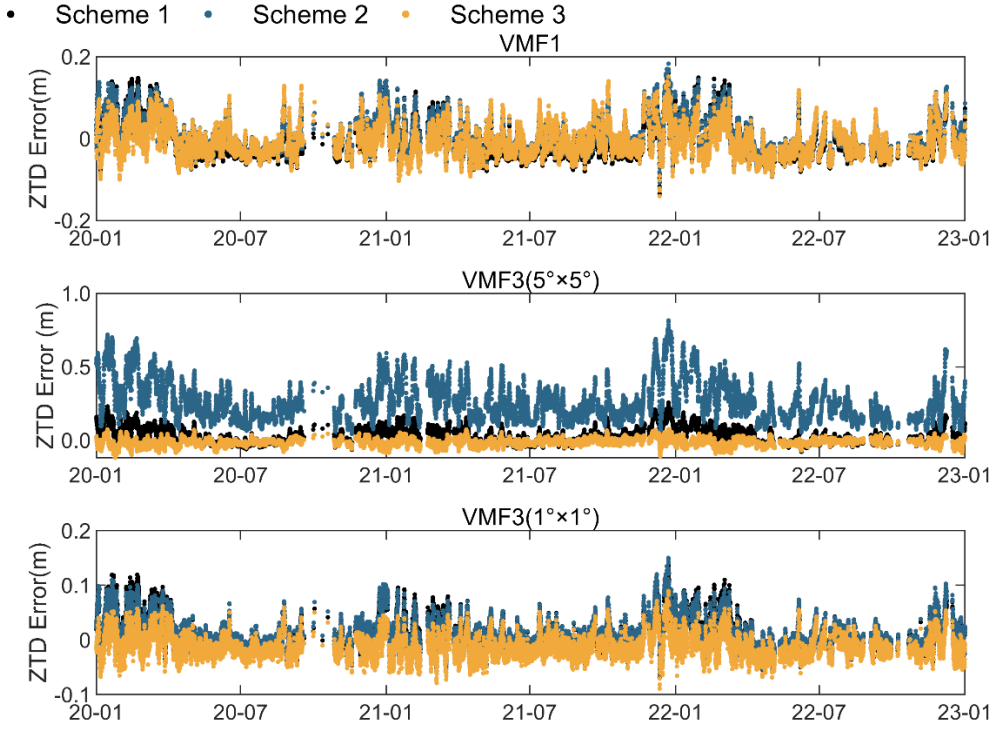

Figure 4 Time series of errors in VMF1/VMF3 predicted ZTD at station IQQE, and the IGS final ZTD product was used as the reference.

5 Conclusions

The ZHD and ZWD provided by grid-based VMF1 and VMF3 tropospheric products are for ground surface values at each grid points, and these products have been widely used for interpolating the *a priori* ZHD and ZWD for GNSS positioning and VLBI stations. In the case that the height of the target GNSS station differs largely from its four surrounding grid points to be used for the interpolation of ZTD, the ZHD and ZWD values at the grid points need to be reduced to the height of the GNSS station before a horizontal interpolation is performed. Since traditional reduction models may not perform well in accuracy, in this study, new ZHD and ZWD reduction models for each of the four grid points to be used for interpolation were developed for an improvement in the accuracy of interpolated results. The sample data for the modeling were the ZHD and ZWD profiles over the grid points obtained from ERA5 monthly averaged reanalysis data during the period of 2010–2019. The two sets of reference data used to evaluate the new models were the ZHD and ZWD at eight pressure levels of radiosonde data at 608 stations and surface ZTD at 394 globally distributed IGS stations during the 3-year period 2020–2022. Test results showed that the accuracy of the ZHD, ZWD, as well as ZTD interpolated from the VMF1/VMF3 products reduced by the new model was significantly better than traditional methods. The new model is expected to be applied in fields such as GNSS positioning and GNSS-meteorology for better performance.

Acknowledgments

This work was funded by the National Natural Science Foundation of China (Grant No. 42361134583, 42274021, 42304015), the Jiangsu Funding Program for Excellent Postdoctoral Talent (Grant No. 2023ZB249), the National Science Centre (NCN) project (Grant No. UMO-2023/48/Q/ST10/00278), the Natural Science Foundation of Henan Province (Grant No. 242300420611), the Construction Program of Space-Air Ground-Well Cooperative Awareness Spatial Information Project (Grant No. B20046), the Independent Innovation Project of "Double-First Class" Construction (Grant No. 2022ZZCX06), and the 2022 Jiangsu Provincial Science and Technology Initiative—Special Fund for International Science and Technology Cooperation (Grant No. BZ2022018). The authors would like to thank the ECMWF, TU Wien, Integrated Global Radiosonde Archive (IGRA) and IGS for providing ERA5 reanalysis data, grid-based VMF1/VMF3 products, radiosonde data and station-wise ZTD products, respectively.

Author contribution

Peng Sun: Conceptualization, Methodology, Investigation, Writing (original draft preparation); **Kefei Zhang:** Funding acquisition, Supervision, Writing (review and editing). **Dantong Zhu**: Formal analysis, Validation. **Shuangshuang Shi:** Investigation, Resources, Visualization. **Xuexi Liu:** Resources, Validation. **Dongsheng Zhao:** Resources. **Minghao Zhang**: Software, **Suqin Wu:** Writing (review and editing).

Competing Interests

The contact author has declared that none of the authors has any competing interests.

Data and Code Availability:

The model developed in this contribution is available at: http://doi.org/10.5281/zenodo.13826894 (Sun, 2024) and GitHub: https://github.com/PengSun1991/VMF_ZTDLpsR, under the MIT License; VMF1 and VMF3 products are available at: http://doi.org/10.17616/R3RD2H(Re3data.Org, 2016); ERA5 monthly averaged reanalysis data are available at : https://doi.org/10.24381/cds.6860a573 (Hersbach et al., 2023); Radiosonde data are available at https://doi.org/10.7289/V5X63K0Q (Durre et al., 2016); IGS ZTD data are available at NASA Crustal Dynamics Data Information System (CDDIS) (International GNSS Service, 2000)

References

Andrei, C.-O. and Chen, R.: Assessment of time-series of troposphere zenith delays derived from the global data assimilation system numerical weather model, GPS Solut., 13, 109–117, https://doi.org/10.1007/s10291-008-0104-1, 2009.

Askne, J. and Nordius, H.: Estimation of tropospheric delay for microwaves from surface weather data, Radio Sci., 22, 379–386, https://doi.org/10.1029/RS022i003p00379, 1987.

Bevis, M., Businger, S., Herring, T. A., Rocken, C., Anthes, R. A., and Ware, R. H.: GPS meteorology: Remote sensing of atmospheric water vapor using the global positioning system, J. Geophys. Res., 97, 15787–15801, https://doi.org/10.1029/92jd01517, 1992.

Boehm, J., Werl, B., and Schuh, H.: Troposphere mapping functions for GPS and very long baseline interferometry from european centre for medium-range weather forecasts operational analysis data, J. Geophys. Res. Solid Earth, 111, n/a-n/a, https://doi.org/10.1029/2005JB003629, 2006.

Boehm, J., Heinkelmann, R., and Schuh, H.: Short note: A global model of pressure and temperature for geodetic applications, J. Geod., 81, 679–683, https://doi.org/10.1007/s00190-007-0135-3, 2007.

Boehm, J., Kouba, J., and Schuh, H.: Forecast Vienna Mapping Functions 1 for real-time analysis of space geodetic observations, J. Geod., 83, 397–401, https://doi.org/10.1007/s00190-008-0216-y, 2009.

Böhm, J., Möller, G., Schindelegger, M., Pain, G., and Weber, R.: Development of an improved empirical model for slant delays in the troposphere (GPT2w), GPS Solut., 19, 433–441, https://doi.org/10.1007/s10291-014-0403-7, 2015.

Chao, C. C.: The tropospheric calibration model for mariner mars 1971, NASA JPL, Pasadena CA, 1974.

Chen, B. and Liu, Z.: A comprehensive evaluation and analysis of the performance of multiple tropospheric models in China region, IEEE Trans. Geosci. Remote Sens., 54, 663–678, https://doi.org/10.1109/TGRS.2015.2456099, 2016.

Chen, G. and Herring, T. A.: Effects of atmospheric azimuthal asymmetry on the analysis of space geodetic data, J. Geophys. Res. Solid Earth, 102, 20489–20502, https://doi.org/10.1029/97JB01739, 1997.

Davis, J. L., Herring, T. A., Shapiro, I. I., Rogers, A. E. E., and Elgered, G.: Geodesy by radio interferometry: Effects of atmospheric modeling errors on estimates of baseline length, Radio Sci., 20, 1593–1607, https://doi.org/10.1029/RS020i006p01593, 1985.

Dousa, J. and Elias, M.: An improved model for calculating tropospheric wet delay, Geophys. Res. Lett., 41, 4389–4397, https://doi.org/10.1002/2014GL060271, 2014.

Durre, I., Yin, X., Vose, R. S., Applequist, S., Arnfield, J., Korzeniewski, B., and Hundermark, B.: Integrated global radiosonde archive (IGRA), version 2.2, https://doi.org/10.7289/V5X63K0Q, 2016.

Hersbach, H., Bell, B., Berrisford, P., Biavati, G., Horányi, A., Muñoz-Sabater, J., Nicolas, J., Peubey, C., Radu, R., Rozum, I., Schepers, D., Simmons, A., Soci, C., Dee, D., and Thépaut, J.: ERA5 monthly averaged data on pressure levels from 1940 to present, https://doi.org/10.24381/CDS.BD0915C6, 2023.

Huang, L., Lan, S., Zhu, G., Chen, F., Li, J., and Liu, L.: A global grid model for the estimation of zenith tropospheric delay considering the variations at different altitudes, Geosci. Model Dev., 16, 7223–7235, https://doi.org/10.5194/gmd-16-7223-2023, 2023.

International GNSS Service: GNSS final troposphere zenith path delay combination product, https://doi.org/10.5067/GNSS/GNSS_IGSTROPZPD_001, 2000.

Jiang, C., Gao, X., Zhu, H., Wang, S., Liu, S., Chen, S., and Liu, G.: An improved global pressure and zenith wet delay model with optimized vertical correction considering the spatiotemporal variability in multiple height-scale factors, Geosci. Model Dev., 17, 5939–5959, https://doi.org/10.5194/gmd-17-5939-2024, 2024.

Kouba, J.: Implementation and testing of the gridded Vienna Mapping Function 1 (VMF1), J. Geod., 82, 193–205, https://doi.org/10.1007/s00190-007-0170-0, 2008.

Kouba, J.: Testing of global pressure/temperature (GPT) model and global mapping function (GMF) in GPS analyses, J. Geod., 83, 199–208, https://doi.org/10.1007/s00190-008-0229-6, 2009.

Lagler, K., Schindelegger, M., Böhm, J., Krásná, H., and Nilsson, T.: GPT2: Empirical slant delay model for radio space geodetic techniques, Geophys. Res. Lett., 40, 1069–1073, https://doi.org/10.1002/grl.50288, 2013.

Landskron, D. and Böhm, J.: VMF3/GPT3: refined discrete and empirical troposphere mapping functions, J. Geod., 92, 349–360, https://doi.org/10.1007/s00190-017-1066-2, 2018.

Leandro, R., Santos, M., and Langley, R. B.: UNB neutral atmosphere models: development and performance, Proceedings of the Institute of Navigation, National Technical Meeting, Institute of Navigation, Monterey, California, USA, 564–573, 2006.

Li, W., Yuan, Y., Ou, J., and He, Y.: IGGtrop_SH and IGGtrop_rH: two improved empirical tropospheric delay models based on vertical reduction functions, IEEE Trans. Geosci. Remote Sens., 56, 5276–5288, https://doi.org/10.1109/TGRS.2018.2812850, 2018.

Möller, G. and Landskron, D.: Atmospheric bending effects in GNSS tomography, Atmospheric Meas. Tech., 12, 23–34, https://doi.org/10.5194/amt-12-23-2019, 2019.

Nafisi, V., Urquhart, L., Santos, M. C., Nievinski, F. G., Bohm, J., Wijaya, D. D., Schuh, H., Ardalan, A. A., Hobiger, T., Ichikawa, R., Zus, F., Wickert, J., and Gegout, P.: Comparison of ray-tracing packages for troposphere delays, IEEE Trans. Geosci. Remote Sens., 50, 469–481, https://doi.org/10.1109/TGRS.2011.2160952, 2012.

Niell, A. E.: Global mapping functions for the atmosphere delay at radio wavelengths, J. Geophys. Res. Solid Earth, 101, 3227–3246, https://doi.org/10.1029/95JB03048, 1996.

Re3data.Org: VMF Data Server, https://doi.org/10.17616/R3RD2H, 2016.

Rüeger, J. M.: Refractive index formulae for radio waves, FIG XXII International Congress, Washington, D.C. USA, 2002.

Saastamoinen, J.: Atmospheric correction for the troposphere and stratosphere in radio ranging satellites, in: The Use of Artificial Satellites for Geodesy, American Geophysical Union (AGU), 247–251, https://doi.org/10.1029/GM015p0247, 1972.

Santos, U. L.: Development of a VMF1-like service at UNB, PhD Thesis, University of New Brunswick, 2011.

Sun, P.: VMF_ZTDLpsR: V1.0.240923, , https://doi.org/10.5281/ZENODO.13826894, 2024.

Sun, P., Zhang, K., Wu, S., Wang, R., and Wan, M.: An investigation into real-time GPS/GLONASS single-frequency precise point positioning and its atmospheric mitigation strategies, Meas. Sci. Technol., 32, 115018, https://doi.org/10.1088/1361-6501/ac0a0e, 2021a.

Sun, P., Zhang, K., Wu, S., Wan, M., and Lin, Y.: Retrieving precipitable water vapor from real-time precise point positioning using VMF1/VMF3 forecasting products, Remote Sens., 13, 3245, https://doi.org/10.3390/rs13163245, 2021b.

Sun, P., Zhang, K., Wu, S., Wang, R., Zhu, D., and Li, L.: An investigation of a voxel-based atmospheric pressure and temperature model, GPS Solut., 27, 56, https://doi.org/10.1007/s10291-022-01390-5, 2023.

Thayer, G. D.: An improved equation for the radio refractive index of air, Radio Sci., 9, 803–807, https://doi.org/10.1029/RS009i010p00803, 1974.

Tregoning, P. and Herring, T. A.: Impact of a priori zenith hydrostatic delay errors on GPS estimates of station heights and zenith total delays, Geophys. Res. Lett., 33, L23303, https://doi.org/10.1029/2006GL027706, 2006.

Wang, J., Balidakis, K., Zus, F., Chang, X., Ge, M., Heinkelmann, R., and Schuh, H.: Improving the vertical modeling of tropospheric delay, Geophys. Res. Lett., 49, e2021GL096732, https://doi.org/10.1029/2021GL096732, 2022.

Wang, X., Zhang, K., Wu, S., He, C., Cheng, Y., and Li, X.: Determination of zenith hydrostatic delay and its impact on GNSS-derived integrated water vapor, Atmospheric Meas. Tech., 10, 2807–2820, https://doi.org/10.5194/amt-10-2807-2017, 2017.

Xia, P., Tong, M., Ye, S., Qian, J., and Fangxin, H.: Establishing a high-precision real-time ZTD model of China with GPS and ERA5 historical data and its application in PPP, GPS Solut., 27, 2, https://doi.org/10.1007/s10291-022-01338-9, 2023.

Yang, F., Guo, J., Li, J., Zhang, C., and Chen, M.: Assessment of the troposphere products derived from VMF data server with ERA5 and IGS data over china, Earth Space Sci., 8, e2021EA001815, https://doi.org/10.1029/2021EA001815, 2021.

Yao, Y., Sun, Z., Xu, C., Zhang, L., and Wan, Y.: Development and assessment of the atmospheric pressure vertical correction model with ERA-Interim and radiosonde data, Earth Space Sci., 5, 777–789, https://doi.org/10.1029/2018EA000448, 2018a.

Yao, Y., Xu, X., Xu, C., Peng, W., and Wan, Y.: GGOS tropospheric delay forecast product performance evaluation and its application in real-time PPP, J. Atmospheric Sol.-Terr. Phys., 175, 1–17, https://doi.org/10.1016/j.jastp.2018.05.002, 2018b.

Yuan, Y., Holden, L., Kealy, A., Choy, S., and Hordyniec, P.: Assessment of forecast Vienna Mapping Function 1 for real-time tropospheric delay modeling in GNSS, J. Geod., 93, 1501–1514, https://doi.org/10.1007/s00190-019-01263-9, 2019.

Zhang, H., Yuan, Y., and Li, W.: An analysis of multisource tropospheric hydrostatic delays and their implications for GPS/GLONASS PPP-based zenith tropospheric delay and height estimations, J. Geod., 95, 83, https://doi.org/10.1007/s00190-021-01535-3, 2021a.

Zhang, H., Yuan, Y., Li, W., Ji, D., and Lv, M.: Implementation of ready-made hydrostatic delay products for timely GPS precipitable water vapor retrieval over complex topography: A case study in the Tibetan Plateau, IEEE J. Sel. Top. Appl. Earth Obs. Remote Sens., 14, 9462–9474, https://doi.org/10.1109/JSTARS.2021.3111910, 2021b.

Zhu, D., Sun, P., Hu, Q., Zhang, K., Wu, S., He, P., Yu, A., Yin, W., and Liu, W.: A fusion framework for producing an accurate PWV map with spatiotemporal continuity based on GNSS, ERA5, and MODIS data, IEEE Trans. Geosci. Remote Sens., 62, 1–14, https://doi.org/10.1109/TGRS.2024.3447832, 2024.

Zus, F., Dick, G., Dousa, J., and Wickert, J.: Systematic errors of mapping functions which are based on the VMF1 concept, GPS Solut., 19, 277–286, https://doi.org/10.1007/s10291-014-0386-4, 2015.